Chemosphere 265 (2021) 129137

Contents lists available at ScienceDirect

Chemosphere

journal homepage: www.elsevier.com/locate/chemosphere

Similar toxicity mechanisms between graphene oxide and oxidized multi-walled carbon nanotubes in *Microcystis aeruginosa*

Edgardo Cruces [a], Ana C. Barrios [b, c], Yaritza P. Cahue [b, c], Brielle Januszewski [b, c], Leanne M. Gilbertson [d, e], François Perreault [b, c, *]

[a] Centro de Investigaciones Costeras Universidad de Atacama, Avenida Copayapu 485, Copiapo, Chile
[b] School of Sustainable Engineering and the Built Environment, Arizona State University, Tempe, AZ, 85287-3005, USA
[c] Nanosystems Engineering Research Center for Nanotechnology-Enabled Water Treatment, United States
[d] Department of Civil and Environmental Engineering, University of Pittsburgh, Pittsburgh, PA, 15261, USA
[e] Department of Chemical and Petroleum Engineering, University of Pittsburgh, Pittsburgh, PA, 15261, USA

HIGHLIGHTS

- Carbon nanotubes and graphene oxide interact differently with cyanobacterial cells.
- Both carbon nanomaterials inhibit growth, photosynthesis, and esterase activity.
- No oxidative stress or membrane damage was observed for both carbon nanomaterials.
- Both carbon nanomaterials induced similar toxicity to *Microcystis aeruginosa*.

GRAPHICAL ABSTRACT

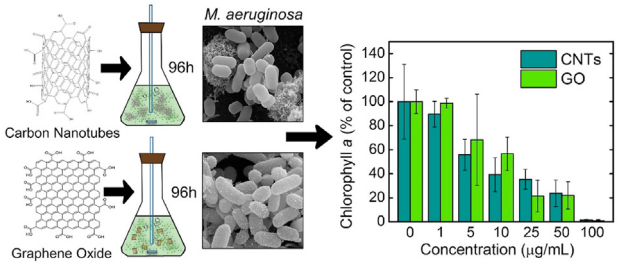

ARTICLE INFO

Article history:
Received 23 September 2020
Received in revised form
25 November 2020
Accepted 26 November 2020
Available online 29 November 2020

Handling Editor: Prof Willie Peijnenburg

Keywords:
Graphene oxide
Carbon nanotubes
Toxicity
Microcystis aeruginosa
Photosynthesis
Oxidative stress

ABSTRACT

In photosynthetic microorganisms, the toxicity of carbon nanomaterials (CNMs) is typically characterized by a decrease in growth, viability, photosynthesis, as well as the induction of oxidative stress. However, it is currently unclear how the shape of the carbon structure in CNMs, such as in the 1-dimensional carbon nanotubes (CNTs) compared to the two-dimensional graphene oxide (GO), affects the way they interact with cells. In this study, the effects of GO and oxidized multi-walled CNTs were compared in the cyanobacterium *Microcystis aeruginosa* to determine the similarities or differences in how the two CNMs interact with and induce toxicity to cyanobacteria. Using change in Chlorophyll *a* concentrations, the effective concentrations inducing 50% inhibition (EC_{50}) at 96 h are found to be 11.1 µg/mL and 7.38 µg/mL for GO and CNTs, respectively. The EC_{50} of the two CNMs were not found to be statistically different. Changes in fluorescein diacetate and 2′,7′-dichlorodihydrofluorescein diacetate fluorescence, measured at the EC_{50} concentrations, suggest a decrease in esterase enzyme activity but no oxidative stress. Scanning and transmission electron microscopy imaging did not show extensive membrane damage in cells exposed to GO or CNTs. Altogether, the decrease in metabolic activity and photosynthetic activity without oxidative stress or membrane damage support the hypothesis that both GO and CNTs induced indirect toxicity through physical mechanisms associated with light shading and cell aggregation. This

* Corresponding author. College Avenue Commons (CAVC) Building, 660 S. College Avenue, #507, Tempe, AZ 85281, USA.
E-mail address: francois.perreault@asu.edu (F. Perreault).

https://doi.org/10.1016/j.chemosphere.2020.129137

indirect toxicity explains why the intrinsic differences in shape, size, and surface properties between CNTs and GO did not result in differences in how they induce toxicity to cyanobacteria.

1. Introduction

Carbon nanomaterials (CNMs) are a family of carbon nanostructures that include the 0-dimensional fullerene, 1-dimensional carbon nanotube (CNTs), and 2-dimensional graphene (Mauter and Elimelech, 2008; Perreault et al., 2015a,b). The exceptional mechanical, electrical, and thermal properties of this class of nanomaterials (NMs) have led to their applications in a wide range of commercial and industrial applications in fields as diverse as electronics (Jariwala et al., 2013), sensors (Peña-Bahamonde et al., 2018), medicine (Loh et al., 2018), photovoltaics (Jariwala et al., 2013), construction (Sanchez and Sobolev, 2010), or water treatment (Perreault et al., 2015a,b; Smith and Rodrigues, 2015). However, this widespread use may ultimately lead to an increased release of CNMs in the environment (Gottschalk et al., 2013). To mitigate the potential risks associated with CNM exposure, a fundamental understanding of the interactions of CNMs with biological systems is needed to guide a safer, more sustainable CNMs development in nano-enabled products (Du et al., 2013; Falinski et al., 2018; Gilbertson et al., 2015).

For CNTs, toxic effects have been shown for a range of organisms, including bacteria, microalgae, invertebrates, and fishes (Falinski et al., 2019; Petersen et al., 2009; Sanchez et al., 2012). In aquatic photosynthetic microorganisms, which are commonly used for ecotoxicological assessment due to their sensitivity, ease of maintenance, and relevance in the aquatic trophic chain, CNTs have been shown to induce growth inhibition and cell death through a variety of mechanisms. Youn et al. showed that gum arabic-stabilized single-walled CNTs inhibit the growth of the green alga *Pseudokirchneriella subcapitata* at concentrations > 0.5 mg/L in a 96 h exposure assay (Youn et al., 2012). Wei et al. showed that, at concentrations ranging between 1 and 10 mg/L, oxidized multi-walled CNTs induced oxidative stress and inhibited photochemical processes at the photosystem II (PSII) level in the green alga *Dunaliella tertiolecta* (Wei et al., 2010). On the other hand, Schwab et al. observed a 96 h EC_{50} value of 1.8 mg/L and 20 mg/L for *Chlorella vulgaris* and *P. subcapitata* exposed to CNTs; however, growth inhibition was primarily (>85%) attributed to a self-shading effect due to light absorption by CNTs, which limited photosynthetic activity (Schwab et al., 2011). Similarly, Long et al. showed that in green alga, *Chlorella* sp., exposed to a concentration inducing a 50% decrease in cell growth (EC_{50}) after 96 h, physical interactions associated with agglomeration and self-shading explained ~50% of the growth inhibition. These results highlight the complexity and variability of CNTs' toxicity in photosynthetic microorganisms, which is attributed to the intrinsic variability in CNTs' properties, such as tube length, diameter, purity, and chirality, differences in the dispersion and exposure conditions, as well as the sensitivity of the different biological models (Bennett et al., 2013; Jiang et al., 2020; Liu et al., 2009).

Similarly, graphene and graphene oxide (GO) have been shown to induce toxicity to multiple biological models (Ahmed and Rodrigues, 2013; Barrios et al., 2019; Falinski et al., 2019; Li et al., 2019). Like CNTs, their toxicity in microalgae appears to be driven by mechanisms associated with oxidative stress, inhibition of photosynthesis, and physical interactions leading to cell death. Tang et al. reported growth inhibition of *Microcystis aeruginosa* at GO concentrations above 10 mg/L, an effect that was associated with the adhesion of GO sheets on the cell surface, the induction of oxidative stress, and the inhibition of the photosynthetic electron transport (Tang et al., 2015). In *Raphidocelis subcapitata*, the growth inhibition 96 h EC_{50} value was found to be ~20 mg/L and was characterized by cell membrane damage, oxidative stress, chlorosis, and physical interactions between the GO sheets and algal cells (Nogueira et al., 2015). Likewise, reduced GO (rGO) exposure in *Scenedesmus obliquus* led to growth inhibition characterized by the cellular deposition of rGO sheets, the inhibition of PSII electron transport, oxidative stress, and lipid peroxidation (Du et al., 2016). However, this effect was observed at much higher concentration than the oxidized form (i.e. GO), with a 72 h EC_{50} value of 148 mg/L. Like for CNTs, differences in the GO properties (Barrios et al., 2019; Faria et al., 2018), exposure conditions, and biological models led to a high variability in the measured toxicity thresholds reported in the literature.

The similarities in toxicological interactions between the 1-D and 2-D forms of CNMs can be explained by their similarities in chemical structure. Indeed, CNTs are essentially rolled-up graphene sheets. However, this morphological change results in important differences in physicochemical properties (Biswas and Lee, 2011; Kauffman and Star, 2010), particularly in water or when the oxidized forms of these materials, such as GO, are considered. For example, GO is an insulating, hydrophilic material that is highly stable in water while CNTs are typically more conductive with reduced stability in water (Dreyer et al., 2010; Qi et al., 2016). Aggregation in aqueous conditions will lead to aggregates of different density, with GO having a more open house-of-cards structure (Ersan et al., 2017). For toxicological interactions, edges and defects, which are found all along the edges in 2-D materials but mainly at the tubes' tip in 1-D CNTs, have been shown to be the main reactive sites for oxidative interactions (Faria et al., 2018; Liu et al., 2011). The distribution of edge sites was also shown to change how CNMs interact with cell membranes, with the penetration of graphene and GO into cell membranes being facilitated by the abundance of sharp irregular edges in the 2-D form (Li et al., 2013; Shi et al., 2011). However, no side-by-side comparison of the toxicity of 1-D CNT and 2-D GO was made for photosynthetic organisms. The variability in doses, materials, and organisms used in toxicity studies makes it hard to determine if the two carbon allotropes share the same mechanisms of toxicity. Similarities can be expected based on their composition, but important differences are also likely due to their different morphologies and physicochemical properties.

In this study, we aimed to determine if the mechanisms of interaction between CNMs and aquatic photosynthetic organisms differ between 1-D and 2-D CNMs. The cyanobacterium *M. aeruginosa* was used as a model organism for toxicity assays due to its ease of culture, sensitivity to environmental contaminants, and frequent use as a model for nano-ecotoxicological studies (Luo et al., 2018; Tang et al., 2015; Wang et al., 2011; Yang et al., 2018). Cyanobacterial cells were exposed to different concentrations of the oxidized forms of two CNMs, oxidized multi-walled CNTs and GO, to provide a better stability in aqueous media. The two CNMs were evaluated at the same biological endpoint, the EC_{50} value, and compared on the basis of change in pigment content,

photosynthetic activity, membrane integrity, and oxidative stress in order to distinguish each CNMs' respective mechanism of toxicity. The results of this work indicate that, despite important differences in how they interact with cells, both GO and CNTs have similar impacts on the physiology of *M. aeruginosa*.

2. Materials and methods

2.1. Chemicals and reagents

A modified Hummer's powdered single layer GO (~99% pure) was purchased from ACS Materials LLC (Medford, MA, USA) and used as received. Multi-walled CNTs (>95% pure) were purchased from CheapTubes (Cambridgeport, VT, USA). The pristine material was acid-treated with nitric acid (HNO_3, 70%) for 4 h under reflux to increase surface oxygen concentrations (Falinski et al., 2019). The fluorescent dyes fluorescein diacetate (FDA), BODIPY™ 493/503 (4,4-difluoro-1,3,5,7,8-pentamethyl-4-bora-3a,4a-diaza-*s*-indacene), and 2′,7′-dichlorodihydrofluorescein diacetate (H_2DCFDA), were obtained from Thermo Fisher Scientific (Molecular Probes, Eugene, OR. All other chemicals were obtained from Sigma-Aldrich (St. Louis, MO, USA). Unless specified, all chemicals were dissolved in deionized (DI) water obtained from a GenPure UV xCAD plus ultrapure water purification system (Thermo Scientific, Waltham, MA).

2.2. Physicochemical material characterization

The morphology and surface chemistry were characterized for each material. For GO sheets, the morphology of the material was visualized by scanning electron microscopy (SEM) using an Amray 1910 FE-SEM operating at an acceleration voltage of 10 eV. Samples were prepared by drop-casting 3 μL of a diluted 50 μg/mL GO stock solution on a 1 cm × 1 cm silicon wafer previously cleaned via UV-ozone treatment for 20 min (UV/Ozone ProCleaner, BioForce Nanosciences, Ames, IA). SEM images were analyzed using the ImageJ v1.50i software to obtain GO dimensions. For CNTs, sizing was done using transmission electron microscope (TEM) images acquired on a Philips CM12 TEM (Philips, Eindhoven, Netherlands) operated at 80 kV. Micrographs were acquired with a Gatan model 791 CCD camera. For TEM imaging, 5 μL of a 50 μg/mL CNTs stock suspension was added to a #160 mesh copper grid (Ted Pella, Redding, CA) and dried under hood conditions.

The surface chemistry of both CNMs was determined by X-ray photoelectron spectroscopy (XPS). For XPS analysis, the sample holder was covered with double-sided copper tape and dusted with enough GO powdered material to cover the surface. The sample was then loaded into a Thermo Scientific ESCALAB 250Xi that uses a monochromatic Al Kα X-ray source with the following parameters: 1486.7 eV, spot size of 650 μm. Survey spectra were collected using a 1.0 eV step size and 150 eV pass energy. Three measurements in different locations were collected per sample. The CasaXPS software version 2.3.23 was used for peak fitting and to calculate the atomic percentage.

The colloidal properties of both CNMs were measured in the Bold Basal Medium (BBM) used for cyanobacterial growth. Suspensions of GO and CNTs were made at a concentration of 180 μg/mL in BBM (pH 6.8) and bath sonicated for 24 h (M3800 Branson Ultrasonic Corporation, Danbury, CT) at a sonication intensity known not to affect the GO sheet size (Perreault et al., 2015a,b). Surface zeta potential and particle hydrodynamic diameter were determined by electrophoretic mobility measurements and dynamic light scattering (DLS) using a NanoBrook ZetaPALS Potential Analyzer (Brookhaven Instrument Corporation). Both hydrodynamic diameter and zeta potential were measured immediately after addition of the CNMs (t = 0 h) or after 96 h, which is the duration of the toxicity experiments.

2.3. Growth inhibition assays

The freshwater cyanobacteria *Microcystis aeruginosa* (UTEX LB 3037) was cultivated in autoclaved Bold Basal Medium (BBM, see Table S1 for composition) at a constant illumination of 4.85 ± 0.31 mW/cm^2 (Thorlabs, NJ, USA) and a controlled temperature of 28 ± 2 °C. This temperature falls within the optimal growth temperature for *M. aeruginosa* (Xu et al., 2012; You et al., 2018). Constant aeration was provided by air bubbling, filtered with a 0.22 μm sterile cellulose filter (VWR, USA), using an aquarium pump (Whisper Air Pump, Tetra, USA). The culture was diluted weekly with fresh BBM medium to maintain a constant algal growth in the stock culture. During culture growth, the relationship between optical density at 750 nm and the cell density was measured by counting cells with a Leica DM6 epifluorescence microscope (Leica Microsystems Inc. Buffalo Grove, IL) in bright field mode with a hemocytometer. The culture was not found to form colonies in the experimental conditions used for toxicity assays.

For CNMs exposure, the algal culture was diluted to 5 × 10^5 cells/mL and allowed to grow until mid-exponential phase (monitored by optical density at 750 nm). Cells were washed three times by centrifugation and resuspension in fresh BBM. Then, the cells were diluted to a final concentration of 2 × 10^6 cells/mL in BBM and 18 mL of culture were added per flasks. From a stock suspensions of GO and CNTs made in deionized (DI) water (2000 μg/mL) and bath sonicated for 72 h (M3800 Branson Ultrasonic Corporation, Danbury, CT), different volumes were added to the cells suspension to reach final CNMs concentrations of 1, 5, 10, 25, 50, and 100 μg/mL. Then, flasks were supplemented, as needed, with fresh autoclaved DI water to have a final total volume in each flask of 20 mL. A negative control (no CNMs) was made by adding 2 mL of sterile DI water into the 18 mL algal dilution. Flasks were kept at a constant temperature (28 ± 2 °C) on a shaker at 60 rpm for 96 h.

2.4. Quantification of photosynthetic pigments

After the 96 h exposure time, 1.5 mL of the algae-CNMs sample was placed in a 2 mL Eppendorf tubes, centrifuged for 10 min at 5000×*g*, and the supernatant was removed. A 0.5 mL volume of methanol was added to the Eppendorf tubes, vortexed, placed on a digital dry bath (Fisher Scientific Waltham, MA) at 70 °C for 10 min, and centrifuged again to pellet the cell debris. A 0.2 mL volume of the supernatant was placed in a transparent microplate to measure chlorophyll *a*, chlorophyll *b*, and total chlorophyll concentrations on a 96 well microplate reader (Synergy H4, BioTek) according to Lichtenthaler (1987).

2.5. Measurement of photosynthetic activity

The polyphasic rise of chlorophyll *a* (Chl *a*) fluorescence in samples (JIP-test) were recorded using a fluorometer (AquaPen-C AP-C 100, Photon Systems Instruments, The Czech Republic). A 3 mL volume of algal sample was placed in cuvettes and kept in darkness for 15 min before Chl *a* fluorescence transient acquisition. Rapid fluorescence induction curves were recorded in the time range between 50 μs and 2 s from the onset of a 3000 μmol photon m^{-2} s^{-1}saturation light, provided by a red-orange light emitting diode at 620 nm. The data obtained from the kinetic curves are: initial fluorescence (F_o), fluorescence yield at 50 μs in which all reaction centers (RCs) in PSII are open, and F_m (maximal

fluorescence), the peak of the fluorescence induction curve where all RCs are closed connecting to accumulation of $Q^-_AQ^{2-}_B$ (Strasser et al., 1995). The maximal PSII quantum yield was evaluated with the parameter F_v/F_m calculated as $F_v/F_m = (F_m - F_o)/F_m$, where F_v is the variable fluorescence (F_m - F_o). The operational PSII quantum yield was evaluated with the parameter F_v'/F_m' calculated as $F_v'/F_m' = (F_m' - F_s)/F_m'$, where F_s is the fluorescence at the steady-state of electron transport, measured under continuous illumination, and F_m' is the maximum fluorescence induced by a saturating light pulse in illuminated steady-state samples. Both the F_v/F_m and the F_v'/F_m' are measured as noted as Qy - Quantum Yield in the AquaPen instrument, with Qy in dark- and light-adapted samples being equivalent to F_v/F_m and F_v'/F_m', respectively.

The photosynthetic characteristics were assessed by electron transport rate (ETR) based on photosynthesis vs. irradiance curves (P–I curves) where Qy is measured as a function of the intensity of actinic irradiance (red-light diode) according to principles described in (Jakob et al., 2005):

$$ETR = Qy \times E \times F_{II} \quad (1)$$

where E is the irradiance, F_{II} is the fraction of absorbed quanta directed to PSII (0.5), which was estimated by determining the fraction of the Chl *a* associated with PSII and its corresponding light harvesting complex. A modified nonlinear function (Jassby and Platt, 1976) was fitted to obtain ETR_{max} (the maximal ETR), α (the initial slope of the P–I curve as an indicator of photosynthetic efficiency) and E_k (the saturating irradiance of photosynthesis).

2.6. EC_{50} determination

The software OriginPro 8.5.1 was used to calculate the half maximum effective concentration (EC_{50}). Data fitting was done using a sigmoidal fit using the dose-response function with the following equation (Chen et al., 2013):

$$y = A1 + \frac{A2 - A1}{1 + 10^{(\log_x 0 - x)p}} \quad (2)$$

Where A1 = bottom asymptote, A2 = top asymptote, $\log_x 0$ = center, p = hill slope, and EC_{50} is given by:

$$EC_{50} = 10^{\log_x 0} \quad (3)$$

2.7. Fluorescent dye assays

Changes in esterase activity, oxidative stress, and lipid peroxidation were evaluated using the fluorescein diacetate (FDA), 2′, 7′-dichlorodihydro fluorescein diacetate (H_2DCFDA), BODIPY™ 493/503 (BODIPY) fluorescent dyes. Stock solution of FDA, H_2DCFDA, and BODIPY were prepared at a concentration of 10 mM (FDA and H_2DCFDA) or 2 mM (BODIPY), according to the manufacturer specification (Molecular Probes™, Thermo Fisher, Waltham, MA), and kept at −20 °C in the dark. After the 96 h exposure, 1 mL of the cyanobacteria cells was stained with a final concentration of 5 mM of FDA, 0.2 mM H_2DCFDA, or 2 mM BODIPY. The samples were incubated for 30 min in the dark before pipetting 200 μL of each sample in a 96 well plate. The fluorescence of FDA and H_2DCFDA were measured on a multi-mode microplate reader (Synergy H1, BioTek) using an excitation wavelength of 490 nm and an emission wavelength of 526 nm, while BODIPY fluorescence was measured using an excitation wavelength of 488 nm and an emission wavelength of 510 nm. Data was expressed as the mean fluorescence intensity and the results as a percentage with respect to the control.

2.8. Electron microscopy of exposed cells

The effect of CNMs exposure on cell morphology was evaluated using SEM and TEM imaging. Cultures were prepared as for the toxicity assays using the 96 h EC_{50} concentration for GO and CNTs. At the end of the 96 h exposure, cells were collected by centrifugation (5000×*g*, 1 min) and the pellet fixed in Karnovsky's fixative (2% paraformaldehyde, 2.5% glutaraldehyde in 0.2 M Sorenson's buffer, pH 7.2) overnight at 4 °C.

For SEM imaging, the fixed cells were washed once with Dulbecco's Phosphate Buffered Saline (DPBS), adhered to poly-L-lysine coated coverslips, and then washed two additional times with DPBS. Secondary fixation was done with 1% OsO_4 in DPBS for 1 h at room temperature, followed by three washes with DI water. Cells were dehydrated with an ascending series of ethanol solutions followed by critical-point drying using a CPD-020 unit (Balzers-Union, Principality of Liechtenstein) with liquid CO_2 as the transition fluid. The dried samples were mounted on aluminum stubs and coated with 10–12 nm of gold-palladium using a Hummer II sputter coater (Technics, San Jose, CA). Imaging was done on a JSM 6300 SEM (JEOL USA, Peabody, MA) operated at 15 kV and images were captured with an IXRF Systems model 500 digital processer (IXRF System, Austin, TX). An average of 20 pictures were taken for each condition, enabling the visualization of over 100 cells per condition.

For TEM imaging, the fixed cells were pelleted and entrapped in 0.8% agarose before washing three times with DPBS. Cell pellets were then fixed with 1% OsO_4 in DPBS for 2 h at room temperature and rinsed four times with deionized water. The cells were stained overnight at 4 °C using 1% aqueous uranyl acetate and washed the following morning with 4 changes of DI water. Cells were dehydrated with an ascending series of ethanol concentrations (20, 40, 60, 80, 100% ethanol), rinsing three times with 100% ethanol. Then, the 100% ethanol was replaced twice with propylene oxide before infiltrating the samples in increasing concentrations of Spurr's standard mixture epoxy resin (Ann Ellis, 2006) using 25% increments. Embedded samples were polymerized at 60 °C for 24 h. Resin blocks with microtomed to 70 nm sections with a Leica Ultracut-R microtome (Leica Microsystems, Buffalo Grove, IL) and collected on formvar-coated copper slot grids. Microtomed sections were stained with 2% uranyl acetate in 50% ethanol for 6 min followed by Sato's lead citrate (Hanaichi et al., 1986) for 3–4 min. Images were obtained using a Philips CM12 TEM (Philips, Eindhoven, Netherlands) operated at 80 kV. Micrographs were acquired with a Gatan model 791 CCD camera. An average of 10 pictures were taken for each condition, enabling the visualization of over 100 cells per condition.

2.9. Data analysis and statistics

Experiments were done in triplicates and data is shown as means and standard deviation, calculated for each treatment. A one-way analysis of variance (ANOVA) followed by a Tukey Honestly Significant Difference (HSD) post-hoc test with $p < 0.05$ was done to determine significant differences between treatments. Significant differences are indicated with lowercase letters in the figures.

3. Results and discussion

3.1. Characterization of carbon nanomaterials

Thorough NM characterization in nanotoxicology studies is essential to understand how the properties of the material can influence its toxicity as well as to make the toxicological data

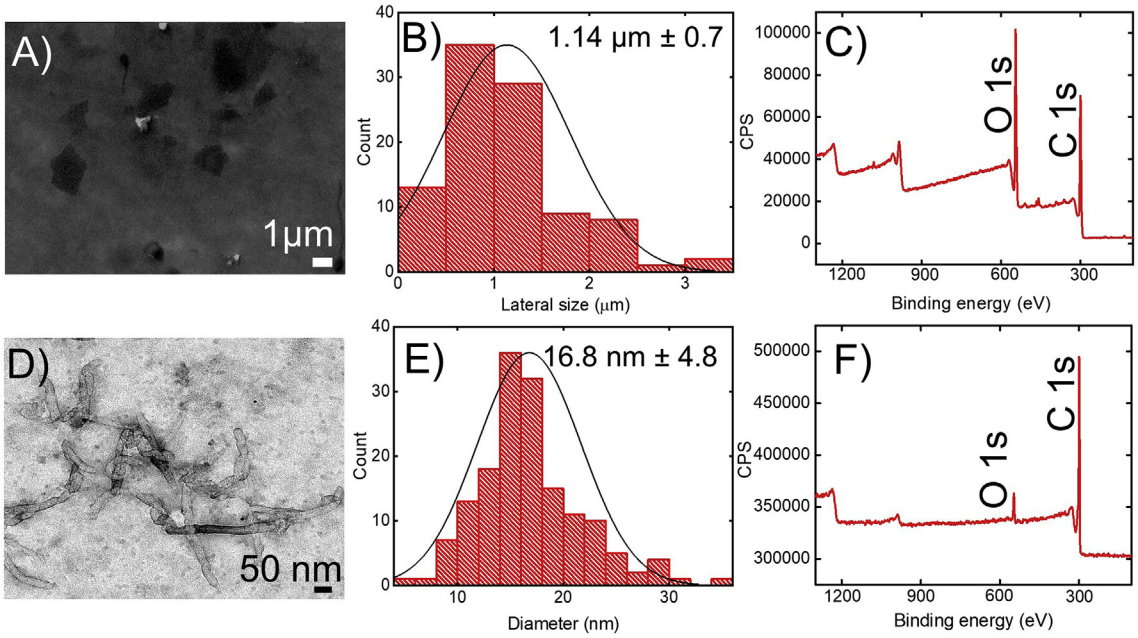

Fig. 1. Characterization of CNMs. Scanning electron micrograph of GO (A); transmission electron micrograph of CNT (D); size distribution of GO (B) and CNTs (E); X-ray photoelectron spectroscopy wide scan spectra of GO (C) and CNTs (F).

generated relevant for other researchers and regulators (Fadeel et al., 2015; Petersen and Henry, 2012). Therefore, the composition, morphology, and size of the GO and CNTs used in this work were characterized using SEM, TEM, and XPS analyses (Fig. 1). SEM imaging of GO showed a material with a typical heterogeneous sheet morphology (Fig. 1A) and an average lateral sheet dimension of 1.14 ± 0.7 μm (Fig. 1B). For CNTs, TEM imaging revealed bundled CNTs with an average tube diameter of 16.8 ± 4.8 nm and a variable tube length of ~0.224 ± 0.083 μm (Fig. 1D and E). For both CNMs, oxidative treatments were used to enhance the dispersibility of the material in the test medium, which is due to the negative charge introduced on the CNTs surface by oxidation. XPS analyses indicate the presence of oxygen in both materials with a C/O ratio for the GO and CNTs of 2.02 and 6.27, respectively (Fig. 1C and F). It should be noted that, due to their structural differences, the same C/O ratio in multi-walled CNTs as in GO is not possible since oxidation affects primarily the outer carbon layer (Datsyuk et al., 2008; Langley et al., 2006). Both CNMs showed initially good dispersibility in the test medium after 24 h of bath sonication. The initial hydrodynamic diameters of GO and CNTs in the BBM medium were of 507 ± 126 nm and 1531 ± 243 nm, respectively (Table 1). Electrophoretic mobility measurements confirmed the negative surface charge of both CNMs, with a zeta potential of −25.81 ± 1.71 mV and −22.49 ± 1.32 mV for GO and CNTs, respectively. This zeta potential value is in the range of previously measured values for these CNMs in complex medium where divalent cations are present (Chowdhury et al., 2015; Skwarek et al., 2016). Divalent cations have been shown to reduce the colloidal stability of NM in suspension, which may lead to their aggregation in the test medium (Chowdhury et al., 2015). This is evidenced by the increase in hydrodynamic diameter after 96 h, the duration of the toxicity tests, in the BBM. For both CNMs, the hydrodynamic diameter is found to increase by one order of magnitude, suggesting high level of aggregation (Table 1). It should be noted that the hydrodynamic diameters shown in Table 1 are calculated based on a spherical particle and therefore are not representative of the real particle size since the intrinsic shape of the materials as well as their aggregate shape are not spherical (Amaro-Gahete et al., 2019; Story et al., 2020). However, the change in hydrodynamic diameter can be used as an indicator of the relative aggregation of CNMs in the medium.

3.2. Growth inhibition dose-response characterization

The toxicity of both CNMs to *M. aeruginosa* was characterized by the decrease in cyanobacterial biomass, measured as extractable Chl *a* concentration, at two different time points, 24 h and 96 h. The use of Chl extraction to measure growth inhibition was due to the optical artefacts introduced by CNMs at high concentrations. Preliminary experiments showed that the presence of the dark-colored CNMs in the test medium led to an artificial decrease in Chl *a* autofluorescence that was not correlated with change in biomass, as evidenced by the significant decrease in Chl *a* autofluorescence at time 0, immediately after addition of CNMs to the cell culture (Fig. S1). This shading effect on Chl *a* autofluorescence was significant at concentrations beyond 10 μg/mL. Similarly, cell counts done by bright field microscopy or flow cytometry were unreliable due to CNMs-cell aggregation (Fig. S1). However, the Chl extraction

Table 1
Characterization of the colloidal behavior of the CNMs suspensions in the BBM medium used for toxicity assays. Asterisks indicate statistical difference between materials, according to a Student's t-test (p = 0.05).

Material	Zeta potential (mV)	Hydrodynamic diameter, 0 h (nm)	Hydrodynamic diameter, 96 h (nm)
GO	−25.81 ± 1.71	507 ± 126	5022 ± 1020
CNTs	−22.49 ± 1.32*	1531 ± 243*	18988 ± 10080*

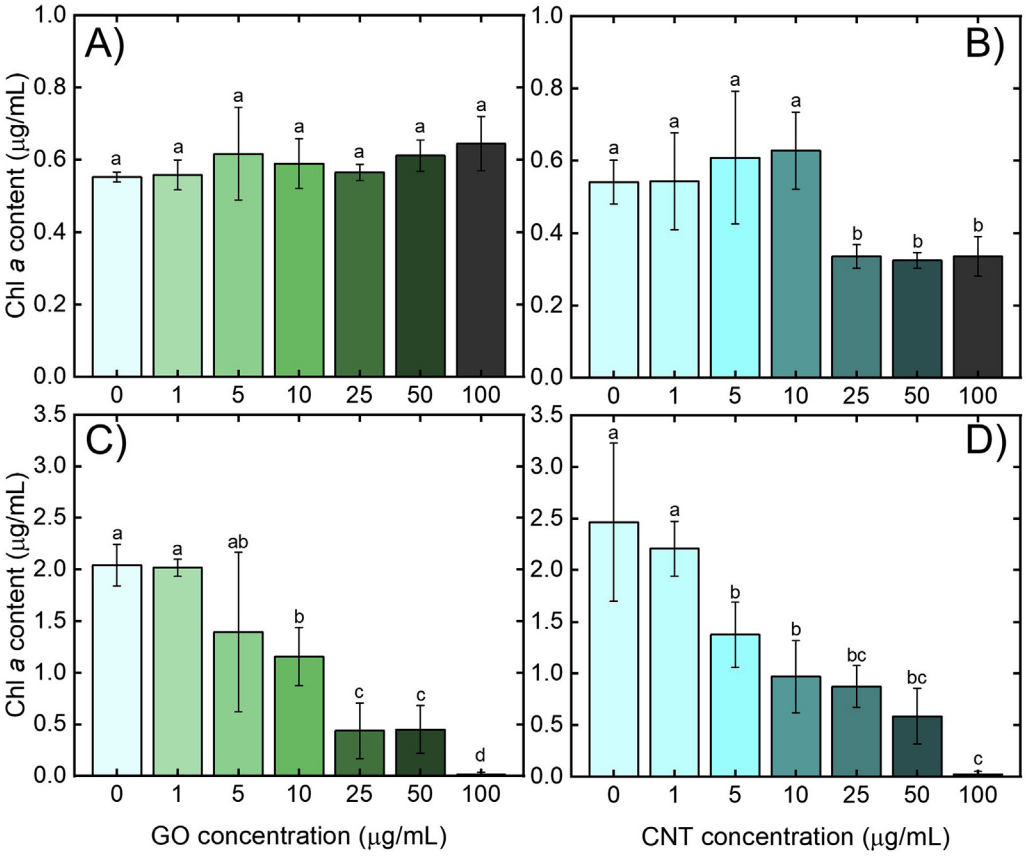

Fig. 2. Change in Chl *a* concentration for *M. aeruginosa* exposed for 24 h (A,B) or 96 h (C,D) to different concentrations of GO (A,C) or CNTs (B,D). Exposures were done under constant illumination and agitation. Data is shown as mean ± standard deviation (n = 3). Letters above the bars represent statistically significant differences between groups, as determined by ANOVA and Tukey's HSD tests (p = 0.05).

procedure separates the pigments from the CNMs (and cells), making this approach more reliable to quantify cyanobacterial biomass in the presence of CNMs.

Exposure of *M. aeruginosa* to CNMs concentration of up to 100 μg/mL did not result in any significant growth inhibition for GO exposure after 24 h of treatment (Fig. 2A). In fact, a small hormetic response, characterized by a stimulation of growth at low exposure concentration, can be observed at 5 and 10 μg/mL. Hormesis is a phenomenon commonly observed in cells exposed to nanomaterials (Agathokleous et al., 2019). However, this effect was not significant due to the variability observed in the treatments, a phenomenon that can be attributed to the complex dynamics of CNMs aggregation in the test media. For CNTs, significant decrease in Chl *a* concentrations was observed at concentrations higher than 25 μg/mL (Fig. 2B). However, Chl *a* concentration decreased to only 60% of the control value and plateaued at this value for up to the highest concentration of 100 μg/mL (Fig. 3B). While this data indicates that CNTs may be more toxic to *M. aeruginosa* after 24 h of exposure, it does not allow for a complete characterization of the dose-response relationship. Therefore, exposure was prolonged to 96 h, where significant growth inhibition could be observed for both GO and CNTs (Fig. 2C and D). Based on the decrease in Chl *a* content at 96 h exposure, EC_{50} values of 11.1 ± 2.4 and 7.38 ± 3.3 μg/mL were calculated for GO and CNTs, respectively (see Fig. S2 for fitted data). Although the EC_{50} value of CNTs is slightly lower than the EC_{50} value of GO, the difference in EC_{50} values is not significant ($p < 0.05$). Therefore, both materials are found to be equally toxic to *M. aeruginosa* after 96 h of exposure.

The EC_{50} values measured in *M. aeruginosa* for GO and CNTs are consistent with previous studies evaluating the toxicity of CNMs to *M. aeruginosa*. For CNT, Wu et al. found a 96 h EC_{50} value of 22 mg/L for single-walled CNTs while, for GO, Xin et al. reported a 96 h EC_{50} value of 52.34 mg/L (Wu et al., 2018; Xin et al., 2018). In a different cyanobacteria model, *Synechococcus elongatus*, the 72 h EC_{50} values for different GO materials ranged from 9.4 to 27.2 mg/L (Malina et al., 2019). When compared to green algae, the EC_{50} values obtained in cyanobacteria are comparable, although there is a large degree of variation between studies. For example, 96 h EC_{50} values of 0.82, 1.8 mg/L and 20 mg/L were found for *Dunaliella tertiolecta*, *C. vulgaris,* and *R. subcapitata* exposed to CNTs (Schwab et al., 2011; Wei et al., 2010). Long et al. found 96 h EC_{50} values ranging from 8 to 45 mg/L for multi-walled CNTs of different lengths and purity in *Chlorella* sp. (Long et al., 2014). For GO, 96 h EC_{50} values ranging from 10-20 mg/L was found in *R. subcapitata* or *S. obliquus* (Hu et al., 2016; Nogueira et al., 2015; Yin et al., 2020; Zhang et al., 2018, 2019). The variability observed in these different studies is explained by the differences in material properties (size, oxygen content, purity, etc.) as well as differences in the biological models and growth conditions used.

3.3. Effect of carbon nanomaterials on photosynthetic activity

To understand how CNMs induced growth inhibition in *M. aeruginosa*, the effect of CNMs exposure on the photosynthetic electron transport, as the primary physiological pathway responsible for biomass production in cyanobacteria, was investigated using Chl *a* fluorescence measurements. Chl *a* fluorescence has been shown to be a sensitive indicator of stress induced by a wide

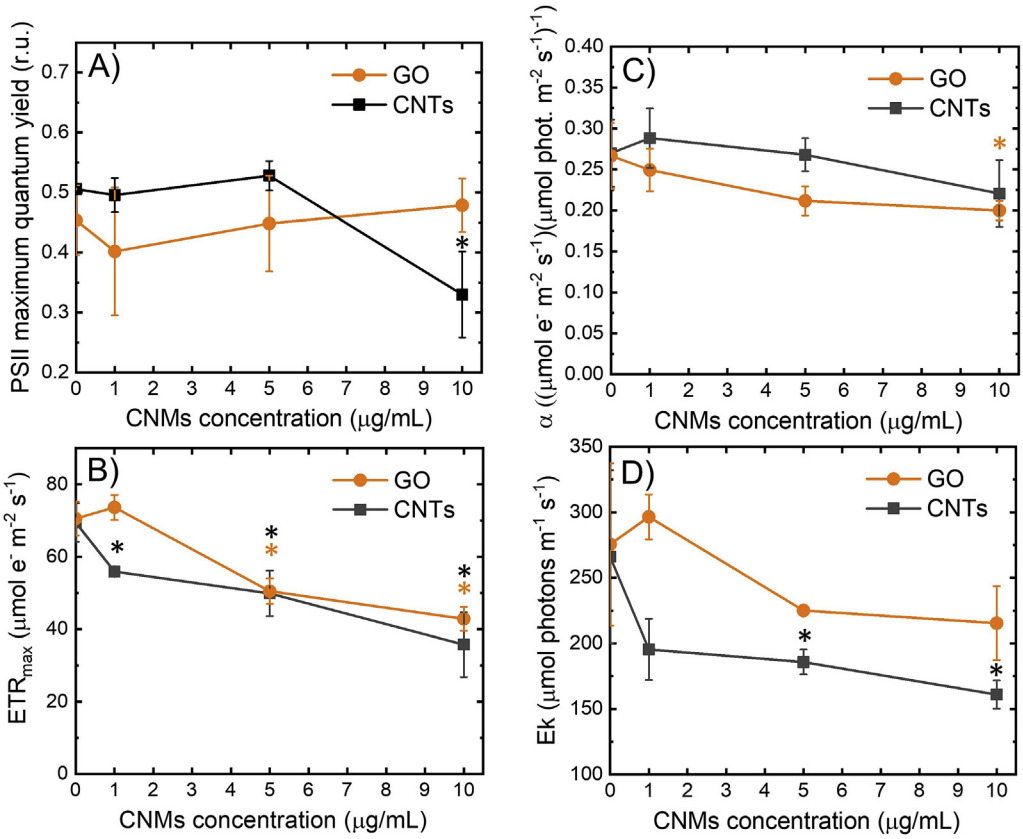

Fig. 3. Change in photosynthetic activity, indicated by the PSII maximal quantum yield for electron transport (A), the maximal photosynthetic electron transport rate (B), the photosynthetic efficiency (C) and the light saturation index (D). These Chl *a* fluorescence parameters were calculated from the P–I light saturation curve in control *M. aeruginosa* cells and in cells exposed 96 h to different concentrations of CNMs. Data is presented as mean ± standard deviation (n = 3). Asterisks above the data points indicate statistical difference compared to the control (p = 0.05), in orange or black for GO or CNT, respectively. (For interpretation of the references to color in this figure legend, the reader is referred to the Web version of this article.)

range of contaminants, including NM, in photosynthetic microorganisms (Chalifour et al., 2016; Dewez et al., 2018; Nguyen et al., 2018a, 2018b; Oukarroum et al., 2017; Zhou et al., 2006). Because of the potential optical artefacts caused by CNMs on Chl *a* fluorescence emission discussed in the previous section, the concentration range was limited to up to 10 μg/mL, which is the threshold concentration beyond which Chl *a* autofluorescence was significantly impacted by light absorption by CNMs (Figure S1).

Exposure of *M. aeruginosa* to both GO and CNTs led to a decrease in photosynthetic electron transport after 96 h of exposure. The effect of both GO and CNTs was less important on the PSII activity than for parameters associated with the steady-state photosynthetic electron transport, which is influenced by processes beyond PSII, such as Photosystem I (PSI) electron transport, CO_2 fixation, and light capture by the light harvesting complexes of PSII and PSI (Cadoret et al., 2004; Harbinson and Foyer, 1991; Miller and Canvin, 1989; Perreault et al., 2009). For example, the PSII maximal quantum yield (F_v/F_m), which indicates the proportion of PSII that are photochemically active, was not significantly affected by GO exposure of up to 10 μg/mL, where it decreased by 35% compared to the control (Fig. 3A). The lack of statistically significant change in F_v/F_m before 10 μg/mL suggests that photoinhibitory damage to the PSII RCs was not the primary mechanism of inhibition (Schansker and Van Rensen, 1999). Conversely, the light saturation curve for *M. aeruginosa* exposed to GO or CNTs revealed that both CNMs had a significant inhibitory effect on the maximum PSII electron transport rate (ETR_{max}) at lower concentrations than F_v/F_m. The ETR_{max} is measured at the steady-state of photosynthetic electron transport and is influenced by changes in PSI electron transport and the carbon fixation pathways (White and Critchley, 1999). In GO, the ETR_{max} decreased by 29% and 40% compared to the control value for 5 and 10 μg/mL, while for CNTs, ETR_{max} decreased to 29% and 49% compared to the control (Fig. 3B). The photosynthetic efficiency, α, decreased by 26% and 19% after 96 h of exposure to 10 μg/mL GO and CNTs, respectively (Fig. 3C), with a significant effect only at 10 μg/mL. Finally, the minimum light demand for the saturation of photosynthesis, E_k, decreased by 22% and 40% for GO and CNTs, respectively, for the same exposure conditions, and was significantly different for the control only for the CNT treatment (Fig. 3D). Altogether, changes in these photosynthetic indicators show less efficient photosynthetic electron transport in *M. aeruginosa* cells in the presence of >5 μg/mL of GO or CNTs. The effect of CNTs on *M. aeruginosa* was slightly more pronounced than for GO, in agreement with the lower EC_{50} value for CNTs.

Changes in photosynthetic activity in microorganisms exposed to CNMs have been attributed to different mechanisms associated with light shading, physical interactions between CNMs and cell leading to agglomeration, membrane damage, and oxidative stress. In the green alga *P. subcapitata*, the toxicity of CNT was primarily driven by agglomeration of algal cells with CNTs as well as a shading effect that decreased the amount of light reaching the light harvesting complexes (Schwab et al., 2011). In GO, it has been observed that the degree of toxicity in algae depends on the internalization through the cell membrane and the generation of reactive oxygen species (Du et al., 2016; Tang et al., 2015).

3.4. Effect of carbon nanomaterials on cellular integrity and oxidative stress

To evaluate the differences in how GO and CNTs induce toxicity to *M. aeruginosa*, the effect of the two materials on *M. aeruginosa*'s physiological response was investigated by comparing both CNMs at their EC_{50} concentration (11.1 ± 2.4 and 7.38 ± 3.3 μg/mL for GO and CNTs, respectively). By doing so, any differences in toxicity that could arise from differences in bioavailability of the CNMs to the cells, such as aggregation and settling, were not considered. The effect of GO and CNTs at their EC_{50} concentration was evaluated using two different fluorescent dyes, H_2DCFDA and FDA, which probe intracellular ROS levels and esterase activity, as a general indicator of cell viability, respectively. Compared to the control samples, both GO and CNTs induced a decrease in the fluorescence emission of FDA and H_2DCFDA suggesting a decrease in metabolic activity and cellular oxidative stress in *M. aeruginosa* cells exposed to CNMs.

Previous studies on the effects of CNMs on microalgae have indicated oxidative stress as one of the interaction mechanisms for both GO and CNTs (Nogueira et al., 2015; Tang et al., 2015; Wei et al., 2010). Therefore, further validation was sought to confirm the trend of lower oxidative stress in CNMs-exposed *M. aeruginosa*. It should be noted that H_2DCFDA fluorescence is dependent on the initial hydrolysis of the dye by the esterase enzymes and a decrease in esterase enzymatic activity, noted by the decrease in FDA fluorescence, may affect the H_2DCFDA fluorescence emission independently of oxidative stress (Barhoumi et al., 2015). Therefore, we used another fluorescent dye, BODIPY, to evaluate potential changes in lipid peroxidation induced by CNMs (Cheloni and Slaveykova, 2013). Using this alternative assay, the absence of oxidative stress in *M. aeruginosa* cells exposed to GO and CNTs is confirmed since the BODIPY fluorescence is not changed compared to the control samples, indicating no change in oxidative damage to the lipids in the presence of CNMs (Fig. 4). The discrepancy between the previous studies mentioned above showing the induction of oxidative stress and this study may be explained by differences in the CNMs' properties, as differences in size, surface chemistry, oxygen content, or presence of oxidation debris (Barrios et al., 2019; Faria et al., 2018; Liu et al., 2011; Perreault et al., 2015a,b; Wang and Gilbertson, 2017) were all shown to influence biological reactivity.

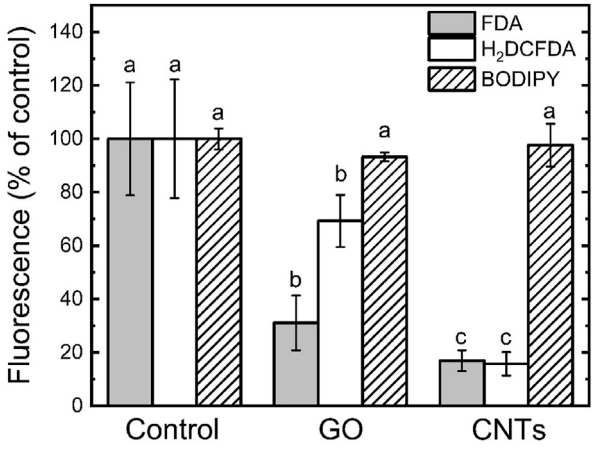

Fig. 4. Change in esterase activity, intracellular oxidative stress, and lipid peroxidation at the 96 h EC_{50} conditions in *M. aeruginosa* exposed to GO or CNTs. Data was normalized to the fluorescence of the control (no NM added) values and error bars represent standard deviation (n = 4). Letters above the bars represent statistically significant differences between groups, as determined by ANOVA and Tukey's HSD tests (p = 0.05).

The decrease in FDA fluorescence induced by CNMs may suggest a decrease in metabolic activity or a disruption of the membrane integrity (Gala and Giesy, 1990; Regel et al., 2002). Because FDA is initially a non-fluorescent apolar molecule that crosses cell membranes passively to be hydrolyzed into the polar and fluorescent fluorescein, it has been considered an indicator of membrane permeability and associated with cell viability in the same way that other polar dyes are used to mark live/dead cells, such as propidium iodide or trypan blue (Altman et al., 1993). However, several studies have shown that changes in the cell metabolism will also affect esterase enzymes activity and consequently FDA fluorescence. For example, FDA fluorescence was found to be correlated with CO_2 fixation and photosynthetic activity in algae (Dorsey et al., 1989). Physiological stresses such as light deprivation or nutrient deficiency can also affect FDA fluorescence by changing the metabolic activity of the cells (Li et al., 2011). Here, the decrease in FDA fluorescence could be explained by the decrease in photosynthetic activity, as shown in Fig. 3, or membrane damage caused by CNMs. Therefore, cellular integrity was evaluated by morphological characterization of CNMs-exposed *M. aeruginosa* cells using electron microscopy imaging.

Cell morphology was evaluated for *M. aeruginosa* cells exposed 96 h to the EC_{50} concentration of GO or CNTs using SEM imaging. When compared to the control cells, which appeared as round and healthy (Fig. 5A), cells exposed to GO sheets show a layer of GO material deposited on the cell surface, which gives the cells a wrinkled surface morphology. All cells visualized on the SEM micrographs of GO-exposed *M. aeruginosa* showed this wrinkled pattern, indicating homogeneous interaction of GO with the cells. On the other hand, CNTs-exposed *M. aeruginosa* cells were not found to be covered in CNTs; instead, the cells appear to be attached to large CNTs aggregates. For both GO- and CNTs-exposed *M. aeruginosa* cells, the cells do not appear to have the collapsed structure indicative of membrane disruption and cell damage that has been observed in previous studies involving the interactions of bacteria with CNMs (Faria et al., 2018; Lu et al., 2017; Perreault et al., 2013) (Fig. 5B and C). This difference may be attributed to the different cell wall architecture between bacteria and cyanobacteria. Indeed, despite being a gram negative prokaryote, *M. aeruginosa* cells possess a thicker peptidoglycan layer that can offer additional protection against membrane damage (Hoiczyk and Hansel, 2000).

The effect of CNMs exposure on the cell morphology was further investigated by analyzing the cellular ultrastructure by TEM imaging (Fig. 5D–F). As in the SEM images, most cells appear to have intact cell membranes for all treatments, although some cells can be seen as having a disrupted cell membrane when in contact with GO or CNTs (Fig. 5E and F, inserts). The control cells have a normal cell physiology with the thylakoids, osmophilic lipid droplets, cyanophicean starch granules, and carboxysomes clearly visible and defined (Fig. 5E) (Martínez-Ruiz and Martínez-Jerónimo, 2018; Song and Qiu, 2007). In comparison, cells exposed to GO or CNTs show a denser and less defined cellular structure and an overall smaller cell size, which suggest reduced metabolic activity. GO sheets are visible around the cyanobacterial cells while, for CNTs, the NM is mostly concentrated in aggregates. Cells are noticeably smaller in CNTs-exposed *M. aeruginosa* samples, supporting an impact on the cell metabolic activity that would impair cell growth.

The absence of significant cell damage, in combination with the limited effect of GO or CNTs on cellular oxidative stress, suggests that a decrease in metabolic activity was the main reason for the reduced growth in CNMs-exposed *M. aeruginosa*. Previous studies using bacterial models have also reported a decrease in microbial activity in GO-entraped cells (Liu et al., 2012; Perreault et al.,

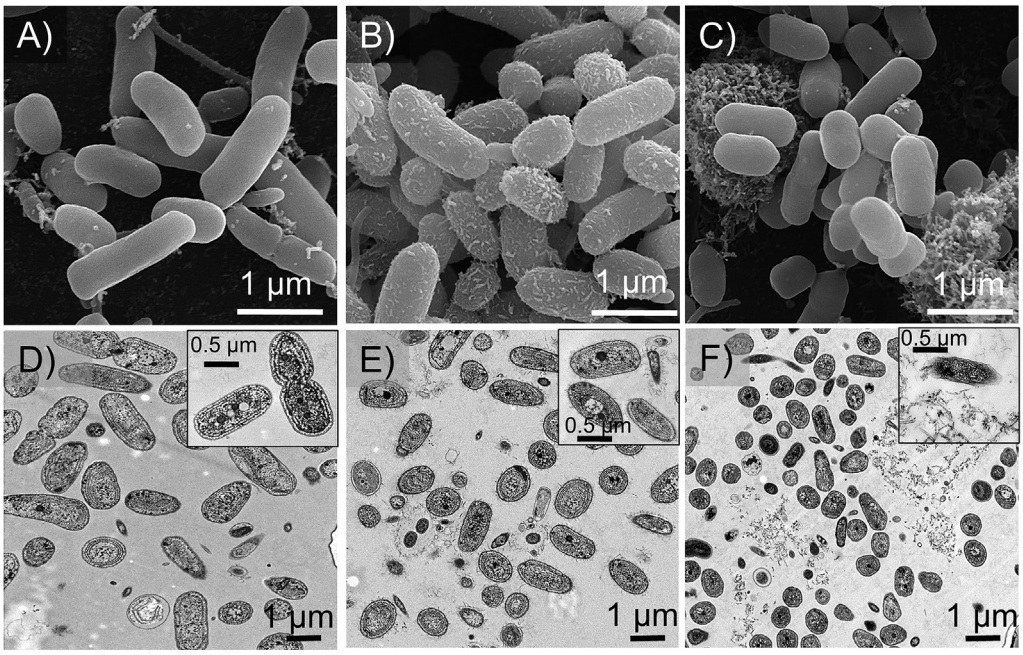

Fig. 5. Scanning electron microscopy (A–C) and transmission electron microscopy (TEM) of control *M. aeruginosa* cells (A,D) or cells exposed to the EC_{50} concentration of GO (B,E) or CNTs (C,F) for 96 h. Inserts in D, E, and F are enlarged pictures of cells representative of the interaction observed.

2015a,b). Reduced metabolic activity is likely due to a decrease in photosynthetic activity, since the cultures were grown photoautotrophically, with photosynthesis as the only source of cellular energy for cell division and growth. Since steady-state photosynthetic electron transport, which is dependent on metabolic activity beyond the photosynthetic electron transport chain, was more sensitive to CNMs' effects than the PSII maximal quantum yield, photoinhibition of PSII may not be a primary mechanism of toxicity of GO and CNTs in cyanobacteria. These results support the findings of Schwab et al., where most of the toxicity of CNTs could be explained by physical mechanisms leading to reduced cell growth, such as aggregation, cell entrapment, and light shading (Schwab et al., 2011). The discrepancies between the current findings and previous reports that suggested that oxidative stress was a major mechanism of interaction for GO or CNTs in microalgae may be explained by differences in the cell architecture of the different models considered, which may have a significant impact on how CNMs interact with cellular systems. Differences in the CNMs surface reactivity, associated with their different size or surface chemistry (Barrios et al., 2019; Perreault et al., 2015a,b; Wang and Gilbertson, 2017), may also explain some of the differences observed between studies, particularly those using the same organism (Tang et al., 2015). To better understand this discrepancy, further studies providing a systematic investigation on the effect of cellular properties and CNMs' surface chemistry will be needed.

4. Conclusion

Despite different physicochemical properties, GO and CNTs appeared to have similar level of toxicity and mechanisms of interaction with the cyanobacterium *M. aeruginosa*. Toxicity of both CNMs was characterized by a decrease in photosynthetic electron transport rate and a decrease in FDA fluorescence, suggesting a reduction in cell metabolic activity. The absence of CNMs-induced oxidative stress and membrane damage in cells exposed to CNMs support the hypothesis of physical interactions leading to reduced photosynthetic and metabolic activity. These physical effects are less dependent on the intrinsic biological reactivity of CNMs than on the way they interact with cells in suspensions, making the differences in surface chemistry or physicochemical properties between the two CNMs less important for their toxicity to cyanobacteria. These findings may be used to develop a general framework to better understand and predict the toxicity of CNMs of different morphologies to cyanobacterial cells.

Credit author statement

E. Cruces: Conceptualization, Supervision, Investigation, Validation, Visualization, Writing- Original draft preparation, Writing-Reviewing and Editing. A.C. Barrios: Conceptualization, Supervision, Investigation, Validation, Visualization, Writing- Original draft preparation, Writing- Reviewing and Editing. Y.P. Cahue: Investigation, Validation, Writing- Reviewing and Editing. B. Januszewski : Investigation, Validation, Writing- Reviewing and Editing. L.M. Gilbertson: Conceptualization, Funding acquisition, Writing-Reviewing and Editing. F. Perreault: Conceptualization, Supervision, Funding acquisition, Writing- Original draft preparation, Writing- Reviewing and Editing.

Declaration of competing interest

The authors declare that they have no known competing financial interests or personal relationships that could have appeared to influence the work reported in this paper.

Acknowledgement

This work was partially funded by the CBET-1708681/1709031 and EEC-1449500 awards of the National Science Foundation, and the Fondo Nacional de Desarrollo Científico y Tecnológico through the FONDECYT award no 11171079. We acknowledge David Lowry for his assistance in sample preparation and acquisition of micrographs and the use of facilities within the Life Science Electron Microscopy Lab and the Eyring Materials Center at Arizona State

University, supported in part by NNCI-ECCS-1542160. We acknowledge Dr. Mark Falinski (Yale University) for donating the carbon nanotube material.

Appendix A. Supplementary data

Supplementary data to this article can be found online at https://doi.org/10.1016/j.chemosphere.2020.129137.

References

Agathokleous, E., Feng, Z.Z., Iavicoli, I., Calabrese, E.J., 2019. The two faces of nanomaterials: a quantification of hormesis in algae and plants. Environ. Int. 131 https://doi.org/10.1016/j.envint.2019.105044.

Ahmed, F., Rodrigues, D.F., 2013. Investigation of acute effects of graphene oxide on wastewater microbial community : a case study. J. Hazard Mater. 33–39. https://doi.org/10.1016/j.jhazmat.2013.03.064.

Altman, S.A., Randers, L., Rao, G., 1993. Comparison of trypan blue dye exclusion and fluorometric assays for mammalian cell viability determinations. Biotechnol. Prog. 9, 671–674. https://doi.org/10.1021/bp00024a017.

Amaro-Gahete, J., Benítez, A., Otero, R., Esquivel, D., Jiménez-Sanchidrián, C., Morales, J., Caballero, Á., Romero-Salguero, F.J., 2019. A comparative study of particle size distribution of graphene nanosheets synthesized by an ultrasound-assisted method. Nanomaterials 9. https://doi.org/10.3390/nano9020152.

Ann Ellis, E., 2006. Solutions to the problem of substitution of ERL 4221 for vinyl cyclohexene dioxide in Spurr low viscosity embedding formulations. Micros. Today 14, 32–33. https://doi.org/10.1017/s1551929500050252.

Barhoumi, L., Oukarroum, A., Taher, L. Ben, Smiri, L.S., Abdelmelek, H., Dewez, D., 2015. Effects of superparamagnetic iron oxide nanoparticles on photosynthesis and growth of the aquatic plant lemna gibba. Arch. Environ. Contam. Toxicol. 68, 510–520. https://doi.org/10.1007/s00244-014-0092-9.

Barrios, A.C., Wang, Y., Gilbertson, L.M., Perreault, F., 2019. Structure – property – toxicity relationships of graphene Oxide : role of surface chemistry on the mechanisms of interaction with bacteria. Environ. Sci. Technol. 53, 14679–14687. https://doi.org/10.1021/acs.est.9b05057.

Bennett, S.W., Adeleye, A., Ji, Z., Keller, A.A., 2013. Stability , metal leaching , photoactivity and toxicity in freshwater systems of commercial single wall carbon nanotubes. Water Res. 47, 4074–4085. https://doi.org/10.1016/j.watres.2012.12.039.

Biswas, C., Lee, Y.H., 2011. Graphene versus carbon nanotubes in electronic devices. Adv. Funct. Mater. 21, 3806–3826. https://doi.org/10.1002/adfm.201101241.

Cadoret, J.C., Demoulière, R., Lavaud, J., Van Gorkom, H.J., Houmard, J., Etienne, A.L., 2004. Dissipation of excess energy triggered by blue light in cyanobacteria with CP43′ (isiA). Biochim. Biophys. Acta Bioenerg. 1659, 100–104. https://doi.org/10.1016/j.bbabio.2004.08.001.

Chalifour, A., LeBlanc, A., Sleno, L., Juneau, P., 2016. Sensitivity of Scenedesmus obliquus and Microcystis aeruginosa to atrazine: effects of acclimation and mixed cultures, and their removal ability. Ecotoxicology 25, 1822–1831. https://doi.org/10.1007/s10646-016-1728-5.

Cheloni, G., Slaveykova, V.I., 2013. The determination of lipid oxidation in chlamydomonas reinhardtii by flow cytometry. Cytometry 83A, 952–961. https://doi.org/10.1002/cyto.22338.

Chen, Z., Bertin, R., Froldi, G., 2013. EC50 estimation of antioxidant activity in DPPH* assay using several statistical programs. Food Chem. 138, 414–420. https://doi.org/10.1016/j.foodchem.2012.11.001.

Chowdhury, I., Mansukhani, N.D., Guiney, L.M., Hersam, M.C., Bouchard, D., 2015. Aggregation and stability of reduced graphene oxide: complex roles of divalent cations, pH, and natural organic matter. Environ. Sci. Technol. 49, 10886–10893. https://doi.org/10.1021/acs.est.5b01866.

Datsyuk, V., Kalyva, M., Papagelis, K., Parthenios, J., Tasis, D., Siokou, A., Kallitsis, I., Galiotis, C., 2008. Chemical oxidation of multiwalled carbon nanotubes. Carbon 46, 833–840. https://doi.org/10.1016/j.carbon.2008.02.012.

Dewez, D., Goltsev, V., Kalaji, H.M., Oukarroum, A., 2018. Inhibitory effects of silver nanoparticles on photosystem II performance in Lemna gibba probed by chlorophyll fluorescence. Curr. Plant Biol. 16, 15–21. https://doi.org/10.1016/j.cpb.2018.11.006.

Dorsey, J., Yentsch, C.M., Mayo, S., McKenna, C., 1989. Rapid analytical technique for the assessment of cell metabolic activity in marine microalgae. Cytometry 10, 622–628. https://doi.org/10.1002/cyto.990100518.

Dreyer, D.R., Park, S., Bielawski, C.W., Ruoff, R.S., 2010. The chemistry of graphene oxide. Chem. Soc. Rev. 39, 228–240. https://doi.org/10.1039/b917103g.

Du, J., Wang, S., You, H., Zhao, X., 2013. Understanding the toxicity of carbon nanotubes in the environment is crucial to the control of nanomaterials in producing and processing and the assessment of health risk for human: a review. Environ. Toxicol. Pharmacol. 36, 451–462. https://doi.org/10.1016/j.etap.2013.05.007.

Du, S., Zhang, P., Zhang, R., Lu, Q., Liu, L., Bao, X., Liu, H., 2016. Reduced graphene oxide induces cytotoxicity and inhibits photosynthetic performance of the green alga Scenedesmus obliquus. Chemosphere 164, 499–507. https://doi.org/10.1016/j.chemosphere.2016.08.138.

Ersan, G., Apul, O.G., Perreault, F., Karanfil, T., 2017. Adsorption of organic contaminants by graphene nanosheets: a review. Water Res. 126, 385–398. https://doi.org/10.1016/j.watres.2017.08.010.

Fadeel, B., Fornara, A., Toprak, M.S., Bhattacharya, K., 2015. Keeping it real: the importance of material characterization in nanotoxicology. Biochem. Biophys. Res. Commun. 468, 498–503. https://doi.org/10.1016/j.bbrc.2015.06.178.

Falinski, M.M., Garland, M.A., Hashmi, S.M., Tanguay, R.L., Zimmerman, J.B., 2019. Establishing structure-property-hazard relationships for multi-walled carbon nanotubes: the role of aggregation, surface charge, and oxidative stress on embryonic zebrafish mortality. Carbon 155, 587–600. https://doi.org/10.1016/j.carbon.2019.08.063.

Falinski, M.M., Plata, D.L., Chopra, S.S., Theis, T.L., Gilbertson, L.M., Zimmerman, J.B., 2018. A framework for sustainable nanomaterial selection and design based on performance, hazard, and economic considerations. Nat. Nanotechnol. 13, 708–714. https://doi.org/10.1038/s41565-018-0120-4.

Faria, A.F., Perreault, F., Elimelech, M., 2018. Elucidating the role of oxidative debris in the antimicrobial properties of graphene oxide. ACS Appl. Nano Mater. 1, 1164–1174. https://doi.org/10.1021/acsanm.7b00332.

Gala, W.R., Giesy, J.P., 1990. Flow Cytometric Techniques to Assess Toxicity to Algae. ASTM Spec. Tech. Publ. https://doi.org/10.1520/stp20110s.

Gilbertson, L.M., Zimmerman, J.B., Plata, D.L., Hutchison, J.E., Anastas, P.T., 2015. Designing nanomaterials to maximize performance and minimize undesirable implications guided by the Principles of Green Chemistry. Chem. Soc. Rev. 44, 5758–5777. https://doi.org/10.1039/c4cs00445k.

Gottschalk, F., Sun, T., Nowack, B., 2013. Environmental concentrations of engineered nanomaterials: review of modeling and analytical studies. Environ. Pollut. 181, 287–300. https://doi.org/10.1016/j.envpol.2013.06.003.

Hanaichi, T., Sato, T., Iwamoto, T., Malavasi-Yamashiro, J., Hoshing, M., Mizuno, N., 1986. A stable lead by modification of Sato's method. J. Electron. Microsc. 35, 304–306.

Harbinson, J., Foyer, C.H., 1991. Relationships between the efficiencies of photosystems I and II and stromal redox state in CO2-free air - evidence for cyclic electron flow in vivo. Plant Physiol. 97, 41–49. https://doi.org/10.1104/pp.97.1.41.

Hoiczyk, E., Hansel, A., 2000. Cyanobacterial cell walls: news from an unusual prokaryotic envelope. J. Bacteriol. 182, 1191–1199. https://doi.org/10.1128/JB.182.5.1191-1199.2000.

Hu, C., Hu, N., Li, X., Zhao, Y., 2016. Graphene oxide alleviates the ecotoxicity of copper on the freshwater microalga Scenedesmus obliquus. Ecotoxicol. Environ. Saf. 132, 360–365. https://doi.org/10.1016/j.ecoenv.2016.06.029.

Jakob, T., Schreiber, U., Kirchesch, V., Langner, U., Wilhelm, C., 2005. Estimation of chlorophyll content and daily primary production of the major algal groups by means of multiwavelength-excitation PAM chlorophyll fluorometry: performance and methodological limits. Photosynth. Res. 83, 343–361. https://doi.org/10.1007/s11120-005-1329-2.

Jariwala, D., Sangwan, V.K., Lauhon, L.J., Marks, T.J., Hersam, M.C., 2013. Carbon nanomaterials for electronics, optoelectronics, photovoltaics, and sensing. Chem. Soc. Rev. 42, 2824–2860. https://doi.org/10.1039/c2cs35335k.

Jassby, A.D., Platt, T., 1976. Mathematical formulation of the relationship between photosynthesis and light for phytoplankton. Limnol. Oceanogr. 21, 540–547. https://doi.org/10.4319/lo.1976.21.4.0540.

Jiang, T., Amadei, C.A., Gou, N., Lin, Y., Lan, J., Vecitis, C.D., Gu, A.Z., 2020. Toxicity of single-walled carbon nanotubes (SWCNTs): effect of lengths, functional groups and electronic structures revealed by a quantitative toxicogenomics assay. Environ. Sci. Nano 7, 1348–1364. https://doi.org/10.1039/d0en00230e.

Kauffman, D.R., Star, A., 2010. Graphene versus carbon nanotubes for chemical sensor and fuel cell applications. Analyst 135, 2790–2797. https://doi.org/10.1039/c0an00262c.

Langley, L.A., Villanueva, D.E., Fairbrother, D.H., 2006. Quantification of surface oxides on carbonaceous materials. Chem. Mater. 18, 169–178. https://doi.org/10.1021/cm051462k.

Li, J., Ou, D., Zheng, L., Gan, N., Song, L., 2011. Applicability of the fluorescein diacetate assay for metabolic activity measurement of Microcystis aeruginosa (Chroococcales, Cyanobacteria). Phycol. Res. 59, 200–207. https://doi.org/10.1111/j.1440-1835.2011.00618.x.

Li, Q., Beier, L.J., Tan, J., Brown, C., Lian, B., Zhong, W., Wang, Y., Ji, C., Dai, P., Li, T., Le Clech, P., Tyagi, H., Liu, X., Leslie, G., Taylor, R.A., 2019. An integrated, solar-driven membrane distillation system for water purification and energy generation. Appl. Energy. https://doi.org/10.1016/j.apenergy.2018.12.069.

Li, Y., Yuan, H., von dem Bussche, A., Creighton, M., Hurt, R.H., Kane, A.B., Gao, H., 2013. Graphene microsheets enter cells through spontaneous membrane penetration at edge asperities and corner sites. Proc. Natl. Acad. Sci. 110, 12295–12300. https://doi.org/10.1073/pnas.1222276110.

Lichtenthaler, H.K., 1987. Chlorophylls carotenoids. Chlorophylls Carotenoids Pigment. Photosynth. Biomembr. 148, 350–382.

Liu, S., Hu, M., Zeng, T.H., Wu, R., Jiang, R., Wei, J., Wang, L., Kong, J., Chen, Y., 2012. Lateral dimension-dependent antibacterial activity of graphene oxide sheets. Langmuir 28, 12364–12372. https://doi.org/10.1021/la3023908.

Liu, S., Wei, L., Hao, L., Fang, N., Chang, M.W., Xu, R., Yang, Y., Chen, Y., 2009. Sharper and Faster " Nano Darts " Kill More Bacteria : A Study of Antibacterial Pristine Single-Walled Carbon Nanotube 3, 3891–3902. https://doi.org/10.1021/nn901252r.

Liu, X., Sen, S., Liu, J., Kulaots, I., Geohegan, D., Kane, A., Puretzky, A.A., Rouleau, C.M., More, K.L., Palmore, G.T.R., Hurt, R.H., 2011. Antioxidant deactivation on graphenic nanocarbon surfaces. Small 7, 2775–2785. https://doi.org/10.1002/smll.201100651.

Loh, K.P., Ho, D., Chiu, G.N.C., Leong, D.T., Pastorin, G., Chow, E.K.H., 2018. Clinical applications of carbon nanomaterials in diagnostics and therapy. Adv. Mater. 30, 1–21. https://doi.org/10.1002/adma.201802368.

Long, Z., Ji, J., Yang, K., Lin, D., Wu, F., 2014. Systematic and quantitative investigation of the mechanism of carbon nanotubes' toxicity toward algae. Environ. Sci. Technol. 48, 4634. https://doi.org/10.1021/es501418w.

Lu, X., Feng, X., Werber, J.R., Chu, C., Zucker, I., Kim, J.-H.H., Osuji, C.O., Elimelech, M., 2017. Enhanced antibacterial activity through the controlled alignment of graphene oxide nanosheets. Proc. Natl. Acad. Sci. 114, E9793–E9801. https://doi.org/10.1073/pnas.1710996114.

Luo, Z., Wang, Z., Yan, Y., Li, J., Yan, C., Xing, B., 2018. Titanium dioxide nanoparticles enhance inorganic arsenic bioavailability and methylation in two freshwater algae species. Environ. Pollut. 238, 631–637. https://doi.org/10.1016/j.envpol.2018.03.070.

Malina, T., Maršálková, E., Holá, K., Tuček, J., Scheibe, M., Zbořil, R., Maršálek, B., 2019. Toxicity of graphene oxide against algae and cyanobacteria: nanoblade-morphology-induced mechanical injury and self-protection mechanism. Carbon N. Y. 155, 386–396. https://doi.org/10.1016/j.carbon.2019.08.086.

Martínez-Ruiz, E.B., Martínez-Jerónimo, F., 2018. Exposure to the herbicide 2,4-D produces different toxic effects in two different phytoplankters: a green microalga (Ankistrodesmus falcatus) and a toxigenic cyanobacterium (Microcystis aeruginosa). Sci. Total Environ. 619–620, 1566–1578. https://doi.org/10.1016/j.scitotenv.2017.10.145.

Mauter, M.S., Elimelech, M., 2008. Environmental applications of carbon-based nanomaterials. Environ. Sci. Technol. 42, 5843–5859. https://doi.org/10.1021/es8006904.

Miller, A.G., Canvin, D.T., 1989. Glycolaldehyde inhibits CO 2 fixation in the cyanobacterium Synechococcus UTEX 625 without inhibiting the accumulation of inorganic carbon or the associated quenching of chlorophyll a fluorescence. Plant Physiol. 91, 1044–1049. https://doi.org/10.1104/pp.91.3.1044.

Nguyen, N.H.A., Padil, V.V.T., Slaveykova, V.I., Černík, M., Ševců, A., 2018a. Green synthesis of metal and metal oxide nanoparticles and their effect on the unicellular alga chlamydomonas reinhardtii. Nanoscale Res. Lett. 13 https://doi.org/10.1186/s11671-018-2575-5.

Nguyen, N.H.A., Von Moos, N.R., Slaveykova, V.I., Mackenzie, K., Meckenstock, R.U., Thűmmler, S., Bosch, J., Ševců, A., 2018b. Biological effects of four iron-containing nanoremediation materials on the green alga Chlamydomonas sp. Ecotoxicol. Environ. Saf. 154, 36–44. https://doi.org/10.1016/j.ecoenv.2018.02.027.

Nogueira, P.F.M., Nakabayashi, D., Zucolotto, V., 2015. The effects of graphene oxide on green algae Raphidocelis subcapitata. Aquat. Toxicol. 166, 29–35. https://doi.org/10.1016/j.aquatox.2015.07.001.

Oukarroum, A., Zaidi, W., Samadani, M., Dewez, D., 2017. Toxicity of nickel oxide nanoparticles on a freshwater green algal strain of chlorella vulgaris. BioMed Res. Int. https://doi.org/10.1155/2017/9528180.

Peña-Bahamonde, J., Nguyen, H.N., Fanourakis, S.K., Rodrigues, D.F., 2018. Recent advances in graphene-based biosensor technology with applications in life sciences. J. Nanobiotechnol. 16, 1–17. https://doi.org/10.1186/s12951-018-0400-z.

Perreault, F., Ait Ali, N., Saison, C., Popovic, R., Juneau, P., 2009. Dichromate effect on energy dissipation of photosystem II and photosystem I in Chlamydomonas reinhardtii. J. Photochem. Photobiol. B Biol. 96, 24–29. https://doi.org/10.1016/j.jphotobiol.2009.03.011.

Perreault, F., de Faria, A.F., Elimelech, M., 2015a. Environmental applications of graphene-based nanomaterials. Chem. Soc. Rev. 44, 5681–5896. https://doi.org/10.1039/c5cs00021a.

Perreault, F., de Faria, A.F., Nejati, S., Elimelech, M., 2015b. Antimicrobial properties of graphene oxide Nanosheets : why size matters. ACS Nano 9, 7226–7236. https://doi.org/10.1021/ascnano.5b02067.

Perreault, F., Tousley, M.E., Elimelech, M., 2013. Thin-film composite polyamide membranes functionalized with biocidal graphene oxide nanosheets. Environ. Sci. Technol. Lett. 1, 71–76. https://doi.org/10.1021/ez4001356.

Petersen, E.J., Akkanen, J., Kukkonen, J.V.K., Weber, W.J., 2009. Biological uptake and depuration of carbon nanotubes by daphnia magna. Environ. Sci. Technol. 43, 2969–2975. https://doi.org/10.1021/es8029363.

Petersen, E.J., Henry, T.B., 2012. Methodological considerations for testing the ecotoxicity of carbon nanotubes and fullerenes: Review. Environ. Toxicol. Chem. 31, 60–72. https://doi.org/10.1002/etc.710.

Qi, Y., Xia, T., Li, Y., Duan, L., Chen, W., 2016. Colloidal stability of reduced graphene oxide materials prepared using different reducing agents. Environ. Sci. Nano 3, 1062–1071. https://doi.org/10.1039/c6en00174b.

Regel, R.H., Ferris, J.M., Ganf, G.G., Brookes, J.D., 2002. Algal esterase activity as a biomeasure of environmental degradation in a freshwater creek. Aquat. Toxicol. 59, 209–223. https://doi.org/10.1016/S0166-445X(01)00254-5.

Sanchez, F., Sobolev, K., 2010. Nanotechnology in concrete - a review. Constr. Build. Mater. 24, 2060–2071. https://doi.org/10.1016/j.conbuildmat.2010.03.014.

Sanchez, V.C., Jachak, A., Hurt, R.H., Kane, A.B., 2012. Biological interactions of graphene-family nanomaterials–an interdisciplinary review. Chem. Res. Toxicol. 15–34.

Schansker, G., Van Rensen, J.J.S., 1999. Performance of active Photosystem II centers in photoinhibited pea leaves. Photosynth. Res. 62, 175–184. https://doi.org/10.1023/a:1006374707722.

Schwab, F., Bucheli, T.D., Lukhele, L.P., Magrez, A., Nowack, B., Sigg, L., Knauer, K., 2011. Are carbon nanotube effects on green algae caused by shading and agglomeration? Environ. Sci. Technol. 45, 6136–6144. https://doi.org/10.1021/es200506b.

Shi, X., Von Dem Bussche, A., Hurt, R.H., Kane, A.B., Gao, H., 2011. Cell entry of one-dimensional nanomaterials occurs by tip recognition and rotation. Nat. Nanotechnol. 6, 714–719. https://doi.org/10.1038/nnano.2011.151.

Skwarek, E., Bolbukh, Y., Tertykh, V., Janusz, W., 2016. Electrokinetic properties of the pristine and oxidized MWCNT depending on the electrolyte type and concentration. Nanoscale Res. Lett. 11 https://doi.org/10.1186/s11671-016-1367-z.

Smith, S.C., Rodrigues, D.F., 2015. Carbon-based nanomaterials for removal of chemical and biological contaminants from water: a review of mechanisms and applications. Carbon N. Y. 91, 122–143. https://doi.org/10.1016/j.carbon.2015.04.043.

Song, Y., Qiu, B., 2007. The CO2-concentrating mechanism in the bloom-forming cyanobacterium Microcystis aeruginosa (Cyanophyceae) and effects of UVB radiation on its operation. J. Phycol. 43, 957–964. https://doi.org/10.1111/j.1529-8817.2007.00391.x.

Story, S.D., Boggs, S., Guiney, L.M., Ramesh, M., Hersam, M.C., Brinker, C.J., Walker, S.L., 2020. Aggregation morphology of planar engineered nanomaterials. J. Colloid Interface Sci. 561, 849–853. https://doi.org/10.1016/j.jcis.2019.11.067.

Strasser, R.J., Srivastava, A., Govindjee, 1995. POLYPHASIC CHLOROPHYLL a FLUORESCENCE TRANSIENT IN PLANTS AND CYANOBACTERIA. Photochem. Photobiol. 61, 32–42. https://doi.org/10.1111/j.1751-1097.1995.tb09240.x.

Tang, Y., Tian, J., Li, S., Xue, C., Xue, Z., Yin, D., Yu, S., 2015. Combined effects of graphene oxide and Cd on the photosynthetic capacity and survival of Microcystis aeruginosa. Sci. Total Environ. 532, 154–161. https://doi.org/10.1016/j.scitotenv.2015.05.081.

Wang, Y., Gilbertson, L.M., 2017. Informing rational design of graphene oxide through surface chemistry manipulations: properties governing electrochemical and biological activities. Green Chem. 19, 2826–2838. https://doi.org/10.1039/c7gc00159b.

Wang, Z., Li, J., Zhao, J., Xing, B., 2011. Toxicity and internalization of CuO nanoparticles to prokaryotic alga microcystis aeruginosa as affected by dissolved organic matter. Environ. Sci. Technol. 45, 6032–6040. https://doi.org/10.1021/es2010573.

Wei, L., Thakkar, M., Chen, Y., Ntim, S.A., Mitra, S., Zhang, X., 2010. Cytotoxicity effects of water dispersible oxidized multiwalled carbon nanotubes on marine alga, Dunaliella tertiolecta. Aquat. Toxicol. 100, 194–201. https://doi.org/10.1016/j.aquatox.2010.07.001.

White, A.J., Critchley, C., 1999. Rapid light curves: a new fluorescence method to assess the state of the photosynthetic apparatus. Photosynth. Res. 59, 63–72. https://doi.org/10.1023/A:1006188004189.

Wu, Y., Wang, Y., Jun, Li, Du, Y. wei, Wang, J. ge, Deng, Z. hong, Huai, S., 2018. Effects of single-walled carbon nanotubes on growth and physiological characteristics of Microcystis aeruginosa. J. Cent. South Univ. 25, 1628–1641. https://doi.org/10.1007/s11771-018-3855-z.

Xin, H., Tang, Y., Liu, S., Yang, X., Xia, S., Yin, D., Yu, S., 2018. Impact of graphene oxide on algal organic matter of microcystis aeruginosa. ACS Omega 16969–16975. https://doi.org/10.1021/acsomega.8b01948.

Xu, K., Jiang, H., Juneau, P., Qiu, B., 2012. Comparative studies on the photosynthetic responses of three freshwater phytoplankton species to temperature and light regimes. J. Appl. Phycol. 24, 1113–1122. https://doi.org/10.1007/s10811-011-9741-9.

Yang, Y., Hou, J., Wang, P., Wang, C., Wang, X., You, G., 2018. Influence of extracellular polymeric substances on cell-NPs heteroaggregation process and toxicity of cerium dioxide NPs to Microcystis aeruginosa. Environ. Pollut. 242, 1206–1216. https://doi.org/10.1016/j.envpol.2018.08.005.

Yin, J., Fan, W., Du, J., Feng, W., Dong, Z., Liu, Y., Zhou, T., 2020. The toxicity of graphene oxide affected by algal physiological characteristics: a comparative study in cyanobacterial, green algae, diatom. Environ. Pollut. 260, 113847. https://doi.org/10.1016/j.envpol.2019.113847.

You, J., Mallery, K., Hong, J., Hondzo, M., 2018. Temperature effects on growth and buoyancy of Microcystis aeruginosa. J. Plankton Res. 40, 16–28. https://doi.org/10.1093/plankt/fbx059.

Youn, S., Wang, R., Gao, J., Hovespyan, A., Ziegler, K.J., Bonzongo, J.C.J., Bitton, G., 2012. Mitigation of the impact of single-walled carbon nanotubes on a freshwater green algae: Pseudokirchneriella subcapitata. Nanotoxicology 6, 161–172. https://doi.org/10.3109/17435390.2011.562329.

Zhang, Y., Meng, T., Guo, X., Yang, R., Si, X., Zhou, J., 2018. Humic acid alleviates the ecotoxicity of graphene-family materials on the freshwater microalgae Scenedesmus obliquus. Chemosphere 197, 749–758. https://doi.org/10.1016/j.chemosphere.2018.01.051.

Zhang, Y., Meng, T., Shi, L., Guo, X., Si, X., Yang, R., Quan, X., 2019. The effects of humic acid on the toxicity of graphene oxide to Scenedesmus obliquus and Daphnia magna. Sci. Total Environ. 649, 163–171. https://doi.org/10.1016/j.scitotenv.2018.08.280.

Zhou, W., Juneau, P., Qiu, B., 2006. Growth and photosynthetic responses of the bloom-forming cyanobacterium Microcystis aeruginosa to elevated levels of cadmium. Chemosphere 65, 1738–1746. https://doi.org/10.1016/j.chemosphere.2006.04.078.